Hardware Prototype of a Time-Encoding Sub-Nyquist ADC

Hila Naaman, *Student Member, IEEE*, Nimrod Glazer, *Member, IEEE*, Moshe Namer, Daniel Bilik, Shlomi Savariego, and Yonina C. Eldar, *Fellow, IEEE*

***Abstract*— Analog-to-digital converters (ADCs) are key components of digital signal processing. Classical samplers in this framework are controlled by a global clock. At high sampling rates, clocks are expensive and power-hungry, thus increasing the cost and energy consumption of ADCs. It is, therefore, desirable to sample using a clock-less ADC at the lowest possible rate. An integrate-and-fire time-encoding machine (IF-TEM) is a time-based power-efficient asynchronous design that is not synced to a global clock. Finite-rate-of-innovation (FRI) signals, ubiquitous in various applications, have fewer degrees of freedom than the signal's Nyquist rate, enabling sub-Nyquist sampling signal models. This work proposes a power-efficient IF-TEM ADC architecture and a sub-Nyquist sampling and FRI signal recovery. Using an IF-TEM, we implement in hardware the first sub-Nyquist time-based sampler, with a detailed hardware design. Our approach provides a robust and accurate method for estimating FRI parameters from IF-TEM data. The proposed hardware and reconstruction technique achieves parameter retrieval with errors up to −25 dB while operating at approximately one-tenth of the Nyquist rate, enabling low-power ADC architectures.**

***Index Terms*— Analog-to-digital conversion, brain-inspired computing, finite-rate-of-innovation (FRI) signals, integrate-and-fire TEM (IF-TEM), sub-Nyquist sampling, time-based sampling hardware.**

I. Introduction

ANALOG-TO-DIGITAL converters (ADCs) are essential electronic components that convert analog signals to digital signals for processing and communication between physical systems and computers [2], [3]. Although synchronous ADCs have been the traditional choice, they come with significant limitations such as high power consumption due to the continuous clock signal, and the need for a stable and accurate clock signal, particularly in high-speed systems where the sampling rate increases, especially in noisy environments [4], [5], [6], [7]. Furthermore, synchronous ADCs require complex clock circuits, which increase the design and implementation complexity [8], [9]. Therefore, innovative ADCs are needed to address these limitations by reducing power consumption and sampling rate while maintaining accuracy and resolution.

One innovative ADC is the asynchronous sigma-delta modulator (ASDM) that can detect changes in input integral and transmit trigger times through linear and nonlinear blocks that consist of an integrator and a Schmitt trigger comparator, respectively [10], [11], [12], [13]. The integrate-and-fire time-encoding machine (IF-TEM) is a special type of ASDM that replaces the Schmitt trigger in the nonlinear block with a set of comparators [11]. IF-TEMs are asynchronous, energy-efficient, and event-driven samplers that use entirely analog, low-power, and small-sized encoders and do not require a global clock [8], [14], [15], [16]. In an IF-TEM, an input signal is integrated, and the resulting signal is compared to a threshold; if the threshold is met, the time instances or their differences are recorded [17], [18], [19], [20], [21]. IF-TEMs have been successfully applied in various applications, such as ultrawideband communication systems, remote sensing, heart activity monitoring, event-based cameras, and spiking neural networks interpretations [22], [23], [24], [25], [26], [27], [28], [29], [30].

In [17], it was first shown that band-limited (BL) signals can be sampled and perfectly recovered by using an IF-TEM. Time-encoding signal reconstruction has been extended to encompass both shift-invariant spaces [31] and finite rate of innovation (FRI) signals [20], [21], [32], [33]. FRI signals, defined by their limited degrees of freedom, enable sub-Nyquist sampling [2], [34]. This property has led to their widespread adoption in various scientific domains, including light detection and ranging [35], ultrasound [36], [37], [38], radar [39], [40], and time-domain optical-coherence tomography [41]. The majority of FRI sampling research exploits signal structure to minimize ADC sampling rates; however, it ignores other aspects of the ADC, such as its power-consuming clock [34], [36], [42], [43]. We address the issue of the synchronous ADCs' power consumption by utilizing the asynchronous IF-TEM sampler, which is energy-efficient.

FRI signal sampling via time-based methods aligns with conventional techniques, notably kernel-based sampling [1], [20], [21], [32], [33], [44]. Naaman et al. in [21] established theoretical guarantees for the sampling and recovery of FRI signals using an IF-TEM and proposed a sampling method that is more robust in the presence of noise than existing

Received 22 August 2024; accepted 12 September 2024. Date of publication 10 October 2024; date of current version 31 October 2024. This work was supported in part by the Estate of Tully and Michele Plesser, in part by the European Research Council (ERC) under the European Union's Horizon 2020 Research and Innovation Program under Grant 101000967, and in part by Israel Science Foundation under Grant 0100101. An earlier version of this paper was presented in part at the International Symposium on Information Theory, ISIT, July 2022 [1]. The Associate Editor coordinating the review process was Dr. Ruqiang Yan. *(Corresponding author: Hila Naaman.)*

The authors are with the Faculty of Mathematics and Computer Science, Weizmann Institute of Science, Rehovot 7610001, Israel (e-mail: hilanaaman10@gmail.com).

Digital Object Identifier 10.1109/TIM.2024.3476568

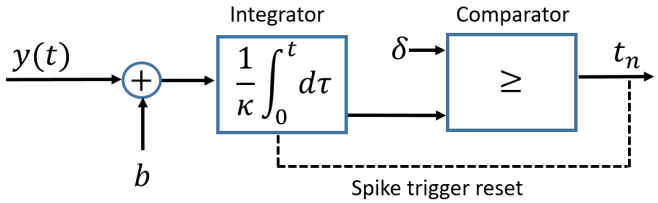

Fig. 1. Diagram of an IF-TEM. The input signal is first biased by b and scaled by κ before being fed into an integrator. Whenever the integrator output reaches the threshold δ, a spike is generated, its time instant is recorded, and the integrator is reset to zero.

techniques. Nonetheless, further enhancements are needed for robust reconstruction when utilizing real hardware data. Our work introduces IF-TEM ADC hardware that demonstrates sub-Nyquist sampling and FRI signal recovery building upon the approach in [21]. We use hardware-measured data with time instances perturbations up to 35 ms. The jittered time instances are modeled as $t_n' = t_n + \epsilon_n$, where t_n are the ideal time instances, and we model the jitter noise as i.i.d. uniformly distributed $\epsilon_n \overset{\text{iid}}{\sim} \mathcal{U}[-\sigma/2, \sigma/2]$. The value of σ depends on the particular system parameters, and in our case, it fluctuates up to 70 ms. This level of timing perturbation can be challenging for current reconstruction techniques to manage. Therefore, the methodology proposed in [21] is modified to ensure robustness in the presence of timing noise inherent in the hardware environment.

Rastogi et al. in [45] implemented an IF-TEM sampler with a refractory period that can accept input signals containing both positive and negative parts over time without biasing the input signal before passing it through the integrator. However, their approach involves two separate paths for the positive and negative parts of the signal and has a refractory period on the order of milliseconds, which poses limitations for measuring FRI signals with shorter periods. To address this limitation and support FRI signals sampling and reconstruction, we propose an improved IF-TEM design with a significantly faster integrator capacitor time in the *ns* range. Furthermore, our solution incorporates a positive bias to the input signal before integration, eliminating the need for a negative path. This streamlined approach reduces the number of components and minimizes heat dissipation. In comparison to the authors' implementation, our solution employs a single comparator with two rules for threshold recognition and trigger of the reset mechanism, along with a straightforward reset mechanism.

Our contributions are twofold. First, we introduce a robust sub-Nyquist sampling and reconstruction technique designed to effectively recover FRI signals below the Nyquist rate while accommodating the inherent noise of hardware. Second, we present a hardware implementation of this technique specifically for FRI signals, which can be employed in low-power time-of-flight applications. To ensure robust recovery of the FRI signals, we prefilter the signal using a sampling kernel that eliminates the signal's dc (zero frequency component). Our reconstruction method relies on both the sampling kernel selection and a new forward model that improves the recovery from noisy hardware data. Compared to our previous work [21], our work offers streamlined proof recovery guarantees based on using a partial sum of the measurements, resulting in robust and stable reconstruction. We demonstrate that our proposed technique outperforms the method in [21] in the presence of noise.

The FRI-TEM hardware prototype we present is designed to accommodate a broad spectrum of FRI signal frequencies and consists of two primary components: an integrator and a reset function. As long as the input signal is positive, the integrator capacitor must operate in its linear domain, which is continuously charged or increasing. In addition, the IF-TEM thresholding requires a rapid reset function, which is achieved by incorporating a differentiator and a field-effect transistor (FET). We demonstrate the capabilities of the system using several FRI signals prefiltered with a BPF filter as the sampling kernel. The designed hardware samples the filtered signal, resulting in consecutive time instance differences, which can be recorded using an oscilloscope or a time-to-digit converter (TDC). To estimate the FRI parameters, we introduce a recovery algorithm that computes the Fourier coefficients and subsequently estimates the parameters using the annihilating filter (AF) techniques. Our findings demonstrate the feasibility of estimating FRI parameters using sub-Nyquist samples, acquired at roughly ten times the rate of innovation, taken at approximately 10 times the rate of innovation, significantly lower than the Nyquist rate of the signal.

The rest of the article is organized as follows. In Section II, we formulate the problem of sampling and recovering an FRI signal using an IF-TEM and discuss some background results. In Section III, we introduce our robust reconstruction algorithm along with simulation results. In Section IV, we justify the required hardware components and explain the circuit challenges. This is followed by a detailed discussion of the analog board's design work specifications. Experimental hardware results of IF-TEM sub-Nyquist sampling and reconstruction are shown in Section V. Finally, we conclude the article in Section VI.

II. Preliminary Results Problem Formulation

In this section, we review some previously established results in time encoding and FRI, followed by our formulation of the theoretical problem of FRI sampling and reconstruction utilizing an IF-TEM sampler.

A. Integrate and Fire Time-Encoding Machine

The IF-TEM operates on principles outlined in [21]. As depicted in Fig. 1, it transforms a bounded input signal $y(t)$ into a series of time instances or spikes and is characterized by positive real parameters b, κ, and δ. The process begins by adding a bias b to the c-bounded signal $y(t)$, where $|y(t)| \leq c < b < \infty$. This sum is integrated and scaled by $1/\kappa$. When the resulting signal reaches the threshold δ, the time instant t_n is recorded, and the integrator resets. This cycle repeats for subsequent time instants, adhering to the relation

$$\frac{1}{\kappa}\int_{t_n}^{t_{n+1}} (y(s) + b)\, ds \;= \delta. \tag{1}$$

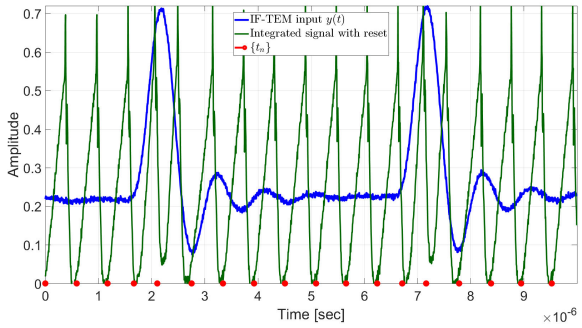

Fig. 2. Our IF-TEM hardware sampling: the IF-TEM input signal $y(t)$ (blue), the integrator output (green), and the IF-TEM time instances (red).

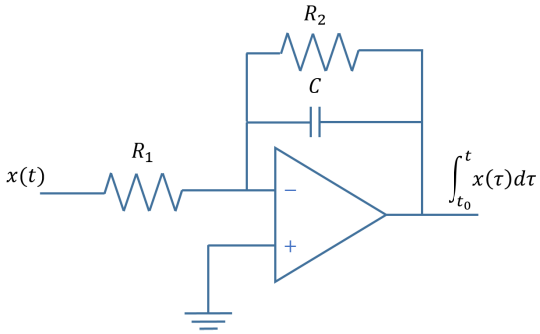

Fig. 3. Hardware integrator circuit. Our hardware implementation is comprised of an operational amplifier, a capacitor C, and resistors R_1 and R_2.

Fig. 2 depicts the operational output of our IF-TEM hardware implementation using real data. The integrator constant κ is determined from the integrator circuit hardware as demonstrated in Fig. 3. The sequence of time encodings $t_n, n \in \mathbb{Z}$ serves as a discrete representation of the continuous-time signal $y(t)$. The goal is to reconstruct $y(t)$ from these encodings. This reconstruction process commonly involves an intermediate step, where we derive another set of discrete values $y_n, n \in \mathbb{Z}$, defined as

$$y_n \triangleq \int_{t_n}^{t_{n+1}} y(s)\,ds \;= -b(t_{n+1} - t_n) + \kappa\delta. \tag{2}$$

The sequence $\{y_n, n \in \mathbb{Z}\}$ are computed from the time-encoding measurements $\{t_n, n \in \mathbb{Z}\}$ and the parameters of the IF-TEM κ, b, and δ. Applying the constraint from (2) and considering that the magnitude of $y(t)$ is bounded by c, we can derive a relationship between consecutive sampling instants [17], [46]

$$\frac{\kappa\delta}{b+c} \le t_{n+1} - t_n \le \frac{\kappa\delta}{b-c}. \tag{3}$$

B. FRI Signal Recovery

Let an FRI signal be characterized as

$$x(t) = \sum_{\ell=1}^{L} a_\ell h(t - \tau_\ell) \tag{4}$$

where $h(t)$ is the pulse shape. The amplitudes $a_\ell \in \mathbb{R}$ and time delays $\tau_\ell \in (0, T]$ constitute the signal's innovation parameters, with L innovations occurring within the interval $(0, T]$. The pulse shape $h(t)$ is assumed to be known and

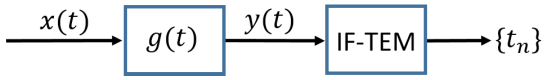

Fig. 4. Continuous-time input signal $x(t)$ is first convolved with the sampling kernel $g(t)$, resulting in the filtered signal $y(t)$, which is then encoded by an IF-TEM, which produces a sequence of nonuniform time instances $\{t_n\}$ representing the signal information.

belongs to $L^2(\mathbb{R})$. The total number of pulses L in the signal is considered to be known a priori. Since the analysis of recovering aperiodic FRI signals using IF-TEM measurements is similar to that of recovering periodic FRI signals [21], in this article, we will concentrate on the scenario of recovering T-periodic FRI signals.

A T-periodic FRI signal can be represented as

$$x(t) = \sum_{n \in \mathbb{Z}} \sum_{\ell=1}^{L} a_\ell h(t - \tau_\ell - nT) \tag{5}$$

where $h(t) \in L^2(\mathbb{R})$ is a prototype pulse. The signal's innovation is characterized by L pairs of amplitudes $a_\ell \in \mathbb{R}$ and delays $\tau_\ell \in (0, T]$. With a rate of innovation $2L/T$, perfect recovery is achievable using $2L$ measurements [2], [34].

Since the signal $x(t)$ is periodic with period T, it can be expressed as a Fourier series

$$x(t) = \sum_{k \in \mathbb{Z}} \hat{x}[k] e^{jk\omega_0 t} \tag{6}$$

where $\omega_0 = 2\pi/T$. The coefficients of the Fourier series (FSCs) are defined as

$$\hat{x}[k] = \frac{1}{T} \hat{h}(k\omega_0) \sum_{\ell=1}^{L} a_\ell e^{-jk\omega_0 \tau_\ell} \tag{7}$$

where $\mathcal{K}$ is a set of integers and $\hat{h}(\omega)$ is the continuous-time Fourier transform of $h(t)$ [2]. Given $k \in \mathcal{K}$, it is presumed that $\hat{h}(k\omega_0) \neq 0$.

The work in [34] demonstrated that the FRI parameters $\{a_\ell, \tau_\ell\}_{\ell=1}^{L}$ can be perfectly recovered from a set of $2L$ FSCs represented as $\hat{x}[k]$. This determination relies on spectral analysis methods, with the AF technique being a notable example, as described in [2]. Consequently, the challenge of reconstructing an FRI signal can be reframed as unambiguously identifying the necessary number of FSCs from the provided signal measurements.

C. Kernel and Sub-Nyquist Sampling

A crucial component of an FRI sampling architecture is the sampling kernel. Generally, sampling kernels that meet the criteria for alias-cancellation to suppress unwanted FSCs [36] with compact support are preferable from a hardware implementation perspective. Based on the robust sampling kernel presented in [21] and to maintain the real-valued nature of the filter response and output, the sampling function $g(t)$ satisfies

$$\hat{g}(k\omega_0) = \begin{cases} 1, & \text{if } k \in \mathcal{K} \\ 0, & \text{else} \end{cases}$$

where $\mathcal{K} = \{-K, \ldots, -1, 1, \ldots, K\}$, and $\hat{g}(k\omega_0)$ denotes the equidistant samples of the signal $g(t)$ Fourier transform, with $K \geq 2L$. A notable instance of this sampling function is the finite-duration sum-of-sincs (SoS) kernel. Its Fourier transform is expressed as

$$\hat{g}(\omega) = \sum_{k\in\mathcal{K}} \operatorname{sinc}\left(\frac{\omega}{\omega_0} - k\right). \tag{8}$$

The resilience of the sampling kernel is a result of selecting a support set $\mathcal{K}$ that is symmetric about zero but does not include zero.

The signal $y(t) = (x * g)(t)$ that represents the filtered output is described as

$$y(t) = \sum_{k\in\mathcal{K}} \hat{x}[k]\hat{g}(k\omega_0)e^{jk\omega_0 t} = \sum_{k\in\mathcal{K}} \hat{x}[k]e^{jk\omega_0 t}. \tag{9}$$

The relationship between the filtered signal samples y_n and the target FSCs is described by the following forward model:

$$y_n = \sum_{k\in\mathcal{K}} \frac{\hat{x}[k]}{jk\omega_0}\left(e^{jk\omega_0 t_{n+1}} - e^{jk\omega_0 t_n}\right). \tag{10}$$

It was shown in [21] that $y(t)$ remains bounded given that $h(t)$ is absolutely integrable and $\max\{a_\ell | a_\ell \in \mathbb{R}\}_{\ell=1}^{L} < \infty$. To extract the FSCs from (10), let

$$\mathbf{y} = \left[\int_{t_1}^{t_2} y(t)dt, \int_{t_2}^{t_3} y(t)dt, \ldots, \int_{t_{N-1}}^{t_N} y(t)dt\right]^\top$$

where N is the number of time instants in the interval T. The measurements $\mathbf{y}$ and the FSCs

$$\hat{\boldsymbol{x}} = \left[-\frac{\hat{x}[-K]}{jK\omega_0}, \ldots, -\frac{\hat{x}[-1]}{j\omega_0}, \frac{\hat{x}[1]}{j\omega_0}, \ldots, \frac{\hat{x}[K]}{jK\omega_0}\right]^\top \tag{12}$$

are related as

$$\mathbf{y} = \mathbf{B}\hat{\boldsymbol{x}} \tag{13}$$

where the matrix $\mathbf{B}$ is defined in (11), as shown at the bottom of the next page. Naaman et al. in [21] have proved that the matrix $\mathbf{B}$ is uniquely left invertible since it has a full column rank. In this case, the Fourier coefficients vector can be calculated as

$$\hat{\boldsymbol{x}} = \mathbf{B}^\dagger \mathbf{y} \tag{14}$$

where $\mathbf{B}^\dagger$ denotes the Moore–Penrose inverse. Perfect reconstruction is established by [21] when $N \geq 4L + 2$ and $|\mathcal{K}| \geq 2L$, as outlined in the theorem below.

Theorem 1 (21, Sect. III-D): Consider an FRI signal $x(t)$ with period T of the form

$$x(t) = \sum_{n\in\mathbb{Z}} \sum_{\ell=1}^{L} a_\ell h(t - \tau_\ell - nT)$$

where L denotes the number of FRI pulses and $h(t) \in L^2(\mathbb{R})$ is a known pulse. Let $x(t)$ be sampled using the mechanism depicted in Fig. 4, with a sampling kernel $g(t)$ satisfying

$$\hat{g}(k\omega_0) = \begin{cases} 1, & \text{if } k \in \mathcal{K} \\ 0, & \text{else} \end{cases}$$

with $\mathcal{K} = \{-K, \ldots, -1, 1, \ldots, K\}$ and $\max_t |(h*g)(t)| < \infty$. The signal $y(t) = (x * g)(t)$ is the result of filtering $x(t)$ with $g(t)$. If the IF-TEM parameters $\{\kappa, \delta, b\}$ chosen to satisfy the condition $b > c$, where $c = \max_t |y(t)|$, and

$$\frac{2K+2}{T} \leq \frac{b-c}{\kappa\delta}. \tag{15}$$

Then, L pairs of amplitudes $a_\ell \in \mathbb{R}$ and delays $\tau_\ell \in (0, T]$ can be perfectly reconstructed using the IF-TEM time instances if:

1) $K \geq L$ when $\{t_\ell\}_{\ell=1}^{L}$ are on-grid and
2) $K \geq 2L$ when $\{t_\ell\}_{\ell=1}^{L}$ are off-grid.

In practice, our IF-TEM hardware circuit introduces noise into the signal, which causes the time occurrences t_n to be perturbed. Consequently, the utilization of the aforementioned algorithm for reconstructing data from hardware measurements led to unstable recovery, as discussed in Section III. Hence, in this article, we introduce a reconstruction strategy designed to offer greater resilience to noise, specifically designed to support the noise inherent in the hardware.

D. Problem Formulation

Consider an FRI signal with period T of the form of (5) and a sampling mechanism as shown in Fig. 4. The signal $x(t)$ undergoes convolution with the sampling kernel $g(t)$, as specified in (8). The resultant signal $y(t)$ is subsequently sampled using an IF-TEM. The amplitude measurements $\{y_n\}_{n=1}^{N}$ represent a discrete representation of $y(t) = (x*g)(t)$, and the time instances $\{t_n\}_{n=1}^{N}$ encodes information of the FRI signal. As our primary aim is to design robust hardware, the FRI parameters $\{a_\ell, \tau_\ell\}_{\ell=1}^{L}$ need to be accurately estimated from the IF-TEM time instances. For this purpose, together with the hardware implementation, a robust recovery algorithm is needed. In Section III, we first introduce our robust recovery mechanism that perfectly recovers the FSCs $\{\hat{x}[k]\}_{k\in\mathcal{K}}$ from the IF-TEM observations in the noiseless case with as few as $4L + 2$ spikes inside an interval T. Then, we illustrate the resilience of our system in the case of noise and demonstrate that it outperforms the one proposed in [21]. In Section IV, we discuss our hardware prototype realizations.

III. Robust Time-Based Sub-Nyquist Sampling and Reconstruction of FRI Signals

The IF-TEM circuit can introduce noise into the signal, which, in turn, can perturb the time instances $\{t_n\}$. Even in the absence of noise, the time instances can only be determined with limited precision. The modeled jittered time instances are expressed as

$$t_n' = t_n + \epsilon_n \tag{16}$$

where t_n are the ideal time instances and $\epsilon_n \overset{\text{iid}}{\sim} \mathcal{U}[-\sigma/2, \sigma/2]$ is the noise jitter. Our hardware experiments have shown that the noise level σ fluctuates up to 70 ms. However, when we attempted to reconstruct FRI signals from IF-TEM measurements using the method presented in our previous work [21], inconsistent recovery was observed with hardware data. Therefore, in this article, we propose a more noise-tolerant reconstruction method that addresses this limitation.

To assess the effectiveness of the new noise-tolerant reconstruction method, we compare it with the approach presented by [21], under the presence of perturbations in the measured time instances. Both methods use a sample kernel without the zero frequency. However, while the method proposed by [21] employs the forward equation specified in (10), our new proposed algorithm adopts an alternative formulation, as introduced in (19) below.

A. Robust Reconstruction

This section presents a method for determining the Fourier coefficients of the FRI signal that is more robust and improves recovery. The reconstruction method presented in [21] and described in Section II relied on calculating the FRI signal $x(t)$ FSCs $\hat{\boldsymbol{x}}$ via (14). In the presence of noise, this causes inaccuracies or deviations in the y_n (10) and $\mathbf{B}$ (11). When calculating the FSCs, the robustness of $\mathbf{B}$, as quantified by its condition number, influences the results. We next demonstrate that by utilizing a partial summation of y_n, perfect recovery is achieved similar to Theorem 1. In the case of noise, our method is more stable. As demonstrated next, when utilizing a partial sum of y_n results in a reconstruction challenge analogous to (14). However, in this scenario, the matrix $\mathbf{A}$ described in (22) takes the place of $\mathbf{B}$. Notably, $\mathbf{A}$ has a better condition number compared to $\mathbf{B}$.

To better understand the reasoning behind this phenomenon, we demonstrate that for every $k \in \mathcal{K}$, utilizing the partial summation of the measurements reduces the noise in each element of $\mathbf{A}$ by half compared to its corresponding element in $\mathbf{B}$. This result is summarized in the following lemma.

Lemma 1: Let $[\mathbf{B}]_{nk} = e^{jk\omega_0 t_{n+1}} - e^{jk\omega_0 t_n}$ be the entries of matrix $\mathbf{B}$, where $n = \{1, \ldots, N-1\}$, $k \in \mathcal{K}$. Let $[\mathbf{A}]_{nk} = e^{jk\omega_0 t_{n+1}}$ be the entries of matrix $\mathbf{A}$, where $n = \{1, \ldots, N-1\}$, $k \in \mathcal{K} \cup \{0\}$. The jittered time instances are modeled as $t_n' = t_n + \epsilon_n$, where t_n are the ideal time instances and the jitter noise is modeled as $\epsilon_n \overset{\text{iid}}{\sim} \mathcal{U}[-\sigma/2, \sigma/2]$, i.i.d. uniformly distributed. For every t_n' and $k \in \mathcal{K}$

$$\operatorname{var}([\mathbf{B}]_{nk}) = 2\operatorname{var}([\mathbf{A}]_{nk}) \tag{17}$$

where var is the variance.

Proof: By utilizing the fact that $t_n' = t_n + \epsilon_n$, and using (11) and (22), it follows that

$$\begin{aligned}\operatorname{var}([\mathbf{B}]_{nk}) &= \operatorname{var}\left(e^{jk\omega_0(t_{n+1}+\epsilon_{n+1})} - e^{jk\omega_0(t_n+\epsilon_n)}\right) \\ &= |e^{jk\omega_0 t_{n+1}}|^2 \operatorname{var}\left(e^{jk\omega_0\epsilon_{n+1}}\right) \\ &\quad + |e^{jk\omega_0 t_n}|^2 \operatorname{var}\left(e^{jk\omega_0\epsilon_n}\right) \\ &= 2\operatorname{var}\left(e^{jk\omega_0\epsilon_n}\right) = 2\operatorname{var}([\mathbf{A}]_{nk})\end{aligned} \tag{18}$$

establishing the lemma. □

It can be intuitively inferred that by utilizing the partial summation, the noise in each element of $[\mathbf{A}]_{nk}$ becomes smaller than the corresponding noise in $[\mathbf{B}]_{nk}$. Consequently, the matrix $\mathbf{A}$ has a better condition number than $\mathbf{B}$. This can be explained by the fact that the condition number of a matrix is a measure of the sensitivity of the matrix to small perturbations in its elements, and a smaller condition number indicates that the matrix is less sensitive to such perturbations. Therefore, by reducing the noise in the elements of $\mathbf{A}$ using the partial summation, we can improve its condition number.

In the subsequent phase, we utilize the partial sum of y_n (10) to introduce a perfect reconstruction condition for FRI signals by using IF-TEM. Rather than extracting the FSCs from y_n via (10) with $\mathcal{K} \in \{-K, \ldots, -1, 1, \ldots, K\}$, where $K \geq 2L$, which establishes the connection between y_n and the FSCs $\hat{x}[k]$, we suggest an alternative approach based on z_n. These z_n values represent the cumulative sums of the measurements y_n defined as

$$z_n = \sum_{i=1}^{n-1} y_i = \sum_{k\in\mathcal{K}} \frac{\hat{x}[k]}{jk\omega_0}\left(e^{jk\omega_0 t_n} - e^{jk\omega_0 t_1}\right) \tag{19}$$

where $n = 2, \ldots, N$. Note that (19) can be written as

$$z_n = \sum_{k\in\mathcal{K}} \frac{\hat{x}[k]}{jk\omega_0} e^{jk\omega_0 t_n} + c \tag{20}$$

where

$$c = -\sum_{k\in\mathcal{K}} \frac{\hat{x}[k]}{jk\omega_0} e^{jk\omega_0 t_1}. \tag{21}$$

Let $\mathbf{z} = [z_2, \ldots, z_N]^{\mathrm{T}} \in \mathbb{R}^{N-1}$ be the vector of partial sums, $\hat{\boldsymbol{z}} = [-(\hat{x}[-K])/jK\omega_0, \ldots, -(\hat{x}[-1])/j\omega_0, c, (\hat{x}[1])/j\omega_0, \ldots, (\hat{x}[K])/jK\omega_0]^{\top} \in \mathbb{C}^{(2K+1)}$ be the vector of FSCs, with c in the zeroth place, and the matrix $\mathbf{A} \in \mathbb{C}^{(N-1)\times(2K+1)}$ is specified as

$$\mathbf{A} = \begin{bmatrix} e^{-jK\omega_0 t_2} & \cdots 1 \cdots & e^{jK\omega_0 t_2} \\ e^{-jK\omega_0 t_3} & \cdots 1 \cdots & e^{jK\omega_0 t_3} \\ \vdots & \ddots & \vdots \\ e^{-jK\omega_0 t_N} & \cdots 1 \cdots & e^{jK\omega_0 t_N} \end{bmatrix}. \tag{22}$$

Consequently, (20) can be represented in matrix form as

$$\mathbf{z} = \mathbf{A}\,\hat{\boldsymbol{z}}. \tag{23}$$

Given that the firings $\{t_n\}_{n=2}^N$ are distinct, and $\mathbf{A}$ is a Vandermonde matrix when $N - 1 \geq 2K + 1$, it follows that $\mathbf{A}$ has full column rank. This means that the matrix $\mathbf{A}$ has linearly independent columns. Therefore, we can perfectly recover the vector of FSCs $\hat{\boldsymbol{z}}$ via

$$\hat{\boldsymbol{z}} = \mathbf{A}^{\dagger}\,\mathbf{z} \tag{24}$$

$$\mathbf{B} = \begin{bmatrix} e^{-jK\omega_0 t_2} - e^{-jK\omega_0 t_1} & \cdots & e^{-j\omega_0 t_2} - e^{-j\omega_0 t_1} & e^{j\omega_0 t_2} - e^{j\omega_0 t_1} & \cdots & e^{jK\omega_0 t_2} - e^{jK\omega_0 t_1} \\ e^{-jK\omega_0 t_3} - e^{-jK\omega_0 t_2} & \cdots & e^{-j\omega_0 t_3} - e^{-j\omega_0 t_2} & e^{j\omega_0 t_3} - e^{j\omega_0 t_2} & \cdots & e^{jK\omega_0 t_3} - e^{jK\omega_0 t_2} \\ \vdots & & \vdots & \vdots & & \vdots \\ e^{-jK\omega_0 t_N} - e^{-jK\omega_0 t_{N-1}} & \cdots & e^{-j\omega_0 t_N} - e^{-j\omega_0 t_{N-1}} & e^{j\omega_0 t_N} - e^{j\omega_0 t_{N-1}} & \cdots & e^{jK\omega_0 t_N} - e^{jK\omega_0 t_{N-1}} \end{bmatrix} \tag{11}$$

where $\mathbf{A}^\dagger$ denotes the Moore–Penrose inverse of $\mathbf{A}$. Once we have $\hat{\boldsymbol{z}}$, the FSCs $\hat{x}[k]$ can be determined uniquely. Using

$$\hat{z}[k] = \begin{cases} -\displaystyle\sum_{k' \in \mathcal{K}} \left(\frac{\hat{x}[k']}{jk'\omega_0} \right) e^{jk'\omega_0 t_1} & \text{if } k = 0 \\ \dfrac{\hat{x}[k]}{j\omega_0 k}, & \text{if } k \in \mathcal{K}\ . \end{cases} \tag{25}$$

The vector of FSCs $\hat{\boldsymbol{z}}$ and the vector of FSCs $\hat{\boldsymbol{x}}$ are related by

$$\hat{\boldsymbol{x}} = \left[\hat{z}[-K], \ldots, \hat{z}[-1], \hat{z}[1], \ldots, \hat{z}[K]\right]^\top \in \mathbb{C}^{2K}. \tag{26}$$

This equation allows us to obtain $\hat{\boldsymbol{x}}$ by selecting the appropriate elements of $\hat{\boldsymbol{z}}$, which is the vector obtained from the partial sums of the measurements. Note that the resulting vector $\hat{\boldsymbol{x}}$ has dimensions $2K$, which implies that it only contains the FSCs for positive and negative frequencies.

Using the vector $\hat{\boldsymbol{z}}$ and (26), the vector of FSCs $\hat{\boldsymbol{x}}$ is uniquely determined. This implies that, excluding the zero-frequency component, the FSCs $\hat{x}[k]$ can be uniquely recovered from the time encodings when $N - 1 \geq 2K + 1$. This indicates that at least $2K + 2$ firing instants within an interval T are needed. As shown in [21], the lowest firing rate using an IF-TEM is $(b - c)/\kappa\delta$. Therefore, to ensure unique reconstruction, the IF-TEM parameters should satisfy the condition $(b - c)/\kappa\delta \geq (2K + 2)/T$ (refer to [21] for further details).

A recovery algorithm to compute the FRI parameters from IF-TEM firings is presented in Algorithm 1. Compared to the technique presented in [21], our method requires the same number of FSCs in the absence of noise. However, in the presence of noise, as is typically the case in real-world hardware, the proposed approach yields a lower error for the same number of measurements.

Algorithm 1 Reconstruction of an FRI Signal With Period T

Input: $N \geq 2K + 2$ spike times $\{t_n\}_{n=1}^N$ in a period T.

Let $n \leftarrow 1$
while $n \leq N - 1$ **do**
  Compute $y_n = \kappa\delta - b(t_{n+1} - t_n)$
  Compute $z_{n+1} = \sum_{i=1}^n y_i$
  $n := n + 1$.
end while
Compute the vector $\hat{\boldsymbol{z}} = \mathbf{A}^\dagger \mathbf{z}$, where $\mathbf{A}$ is defined in (22)
Compute the Fourier coefficients vector $\hat{\boldsymbol{x}}$ from $\hat{\boldsymbol{z}}$ using (26)
Estimate $\{a_\ell, \tau_\ell\}_{\ell=1}^L$ via a spectral analysis method for $K \geq 2L$.

Output: $\{(a_\ell, \tau_\ell)\}_{\ell=1}^L$.

B. Numerical Evaluation

This section presents simulation results that validate the effectiveness of Algorithm 1 and demonstrate how the proposed reconstruction technique improves the conditioning of the forward transformation. This leads to significantly better reconstruction accuracy, which is crucial for precise signal recovery in real hardware implementations. To test Theorem 1, we simulate an FRI signal $h(t)$ consisting of Dirac impulses

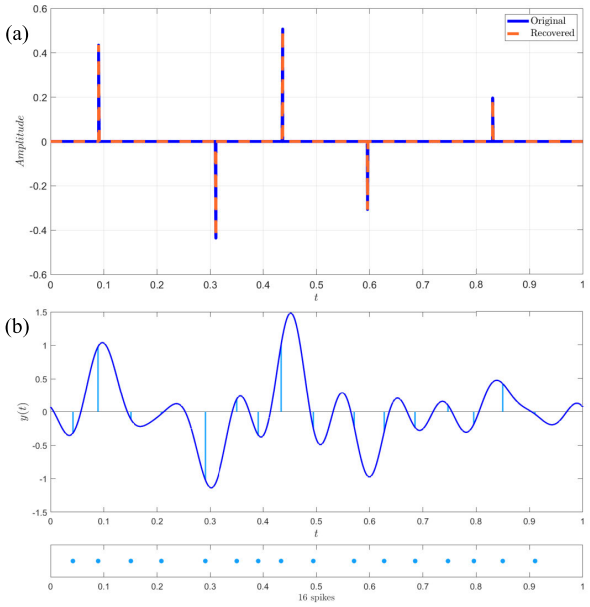

Fig. 5. IF-TEM sampling with a modified kernel enables perfect recovery of an FRI signal. (a) Original input signal with $L = 5$ pulses and its reconstructed version. (b) Filtered signal $y(t)$ along with the IF-TEM firing times t_n.

with period $T = 1$ s and $L = 5$ pulses. The pulse amplitudes are randomly selected between $[-1, 1]$ and the time delays are chosen randomly from the interval $(0, 1)$ using a grid with a resolution of 0.05 The input $x(t)$ is processed through SoS kernel with $\mathcal{K} = \{-K, \ldots, -1, 1, \ldots, K\}$, with K equal to L. The resulting filtered signal $y(t)$ is input to an IF-TEM. The IF-TEM's parameters are chosen to satisfy the bound in (15). For this setup, the IF-TEM produced 16 firing events per period, shown in Fig. 5(b). Fig. 5(a) shows that using a kernel without zero frequency enables perfect FRI signal recovery.

Since the IF-TEM circuit introduces noise that perturbs the firing times $\{t_n\}$, we analyze recovery under jitter: $t'_n = t_n + \epsilon_n$, as in (16). We compare our method to the algorithm from [21], both using kernels without zero frequency. While [21] uses the forward relation in (10), we employ a different one defined in (19).

The forward operators $\mathbf{A}$ and $\mathbf{B}$ [(13) and (23)] are used to recover the FRI signals in each method. These matrices depend on the measured firing times and sampling kernel. Fig. 6 compares the condition numbers of $\mathbf{A}$ and $\mathbf{B}$ as a function of L, using $4L + 2$ perturbed firing times. Results are averaged over 5000 random monotonic time sequences $t_n \in [0, T)_{n=1}^N$. Matrix $\mathbf{A}$ consistently has a lower condition number than $\mathbf{B}$, indicating that our reconstruction algorithm improves stability and noise resilience.

We evaluate the relative MSE in estimating time delays to compare reconstruction accuracy between our algorithm and [21]

$$\text{MSE} = 10 \log \left(\sum_{\ell=1}^{L} (\tau_\ell - \hat{\tau}_\ell)^2 \right). \tag{27}$$

Here, $x(t)$ is an FRI signal as in (5) with period $T = 1$ s, $L = 3$ pulses, and $h(t)$ a cubic B-spline of order 3. The off-grid amplitudes $\{a_\ell\}_{\ell=1}^3$ and delays $\{\tau_\ell\}_{\ell=1}^3$ are randomly

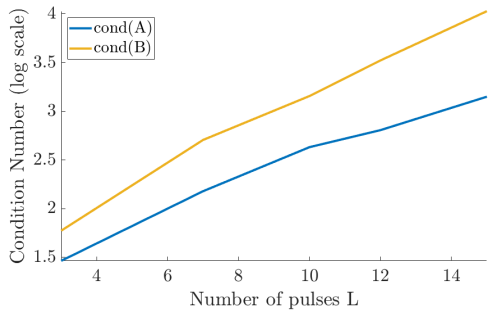

Fig. 6. Mean conditioning of matrices A and B, plotted with respect to the quantity of FRI pulses, L.

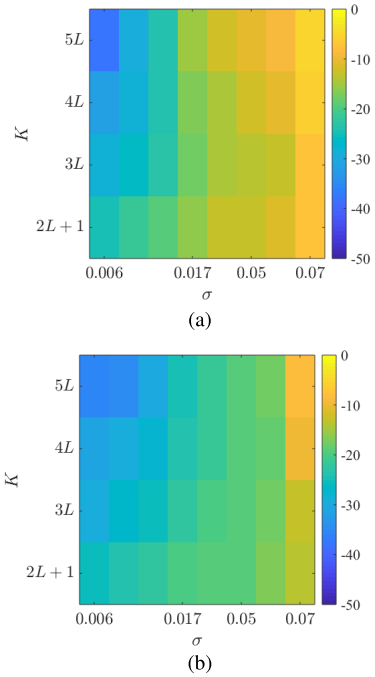

Fig. 7. Comparison of [21] and Algorithm 1 for off-grid time delays with perturbation in the time encodings: our method has lower error compared to [21]. (a) Without zero approach in [21]. (b) Without zero Algorithm 1.

drawn from $[1, 5]$ and $(0, T]$. The IF-TEM parameters are $b = 2.5c$ with $c = \max_t |y(t)|$, $\kappa = 1$, and δ satisfies (15). An SoS kernel with $\mathcal{K} = \{-K, \ldots, -1, 1, \ldots, K\}$ computes the FSCs $\hat{x}[k]$. The firing times $\{t_n\}$ are perturbed as $t'_n = t_n + \epsilon_n$ with ϵ_n uniform on $[-\sigma/2, \sigma/2]$. We estimate time delays using an AF with Cadzow denoising, which needs $>2L$ consecutive FSCs, so we set $K \geq 2L + 1$ excluding zero. Our method calculates $\{\hat{x}[k]\}_{k=-K}^{-1}$ and $\{\hat{x}[k]\}_{k=1}^{K}$, by applying Cadzow denoising independently to every sequence and then jointly estimate delays via block annihilation [47].

Fig. 7 shows delay estimation MSEs for varying numbers of FSCs and noise levels, averaged over 500 realizations. Fig. 7(a) and (b) compares [21] and Algorithm 1 without zero frequency for $K \in [2L + 1, 5L]$. We observe gains up to 10 dB for our method. Since the jitter of the time encoding is equivalent to quantization noise, the lower MSEs suggest our method can operate using fewer bits than [21].

IV. Analog Board and Hardware Challenges

In this section, we will describe the specifications of our FRI-TEM hardware prototype.

A. FRI-TEM Analog Board

We begin by discussing the key components of the FRI-TEM hardware implementation, as well as various circuit design considerations. As shown in Figs. 8 and 9, the analog board comprises three sequential stages: the generation of an FRI signal, bandpass filtering, and an IF-TEM sampler.

The FRI signal generator uses an analog approach, which is known for its low digital noise and ability to accurately simulate real-world applications such as radar and ultrasound [48]. The process of signal production involves several components working together to generate and process a signal. For instance, in creating an FRI signal that contains two pulses, one feasible configuration involves employing a signal generator comprising a scope, a splitter, an analog delay generator, and a passive radio frequency (RF) combiner. The scope generates an FRI pulse (10–500 ns wide) that is transmitted through the splitter. The splitter receives the pulse and sends it to both the delay generator and the combiner (see Fig. 8). The delay generator is comprised of a fiber-optic cable, a photo-diode encoder, and a photo-diode detector. Encoding the signal with the photo-diode encoder is the initial step of the delay generator. The signal then travels through the fiber-optic line, causing a delay of at least 4 μs. The significance of the fiber-optic delay implementation originates from its well-known benefits, such as the introduction of low digital noise, which more accurately simulates practical applications. To decode the delayed input signal, a photo-diode detector is used to transform the signal to an analog signal with the same frequency as the original FRI input pulse. In Fig. 8, for instance, the FRI signal $x(t)$ (5) consists of two 20-MHz pulses separated by a relative delay of 4 μs. The output of the combiner, $x(t)$, is then sent as input to the sampling kernel.

The filter, also known as the sampling kernel, is used to remove the dc component of the signal, as shown in Fig. 10. For example, if the frequency of the signal is 10 Hz, the magnitude of the zero-frequency component would be -30 dB. The positioning of the sampling kernel is critical for time-based FRI signals using an IF-TEM (see Section III). Since our objective of employing a compactly supported filter is to eliminate the dc component, we utilize a BPF in the hardware setup.

To accurately recover and analyze two pulses of an FRI signal within a noise-free setting for a short time period such as $T = 10$ μs, the minimum theoretical sampling rate required is 0.4 MHz [2], [34]. To facilitate this fast sampling and reconstruction process, a 0.22 kHz–1 MHz BPF was chosen. As shown in Fig. 10, an eighth-order BPF is employed, enabling a suitable tradeoff between energy usage and reconstruction performance.

The output of the filter, $y(t)$ (9), is then transmitted to the IF-TEM sampler. The block diagram of the IF-TEM circuit is shown in Fig. 9, the specific components list of the IF-TEM circuit can be found in Table I. A prototype of the IF-TEM

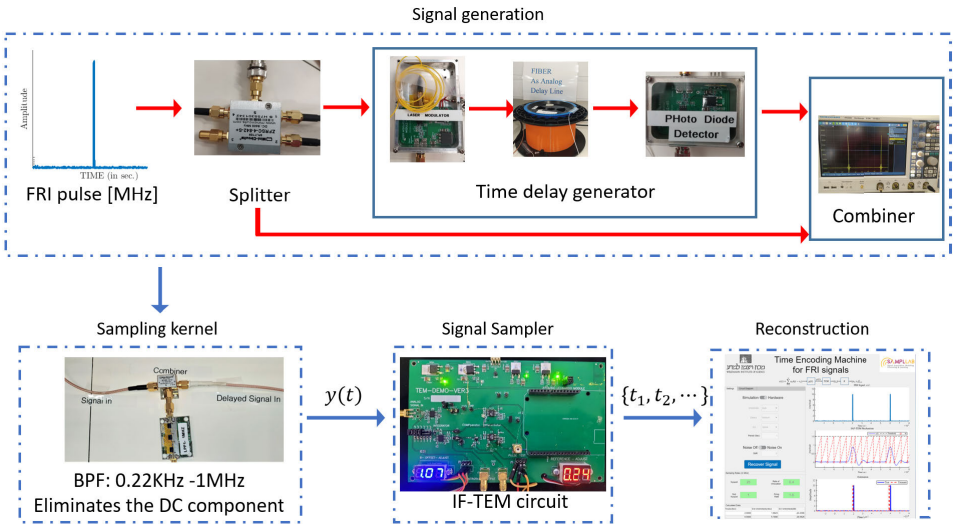

Fig. 8. FRI-TEM hardware prototype includes a signal generator, a sampling kernel, and an IF-TEM sampler. In the case of FRI signals consisting of two pulses, the signal generator is configured as follows: a delay path of 4 μs is constructed using a modulator optic fiber terminating in a photo-diode detector. Then, a combiner receives the original signal (single one or more) from the generator and the delayed path to create the FRI signal. The generated signal is passed into a BPF of 0.22 kHz–1 MHz which removes the zero frequency. Lastly, the IF-TEM sampler board samples the processed signal. Based on Algorithm 1, the FRI signal is recovered.

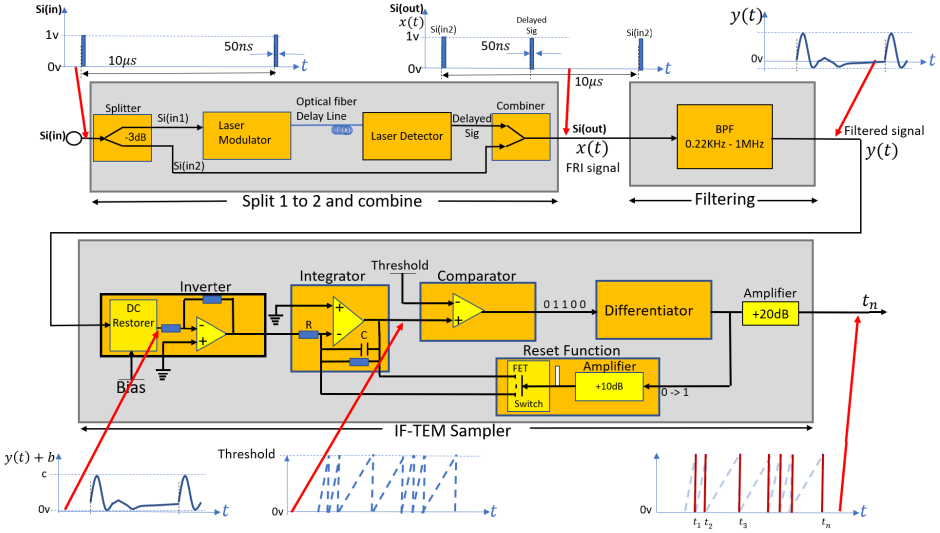

Fig. 9. Block diagram of the analog board. In the example, the signal generator is configured to produce FRI signals comprising two pulses, yet the hardware configuration is adaptable to accommodate any FRI signal form.

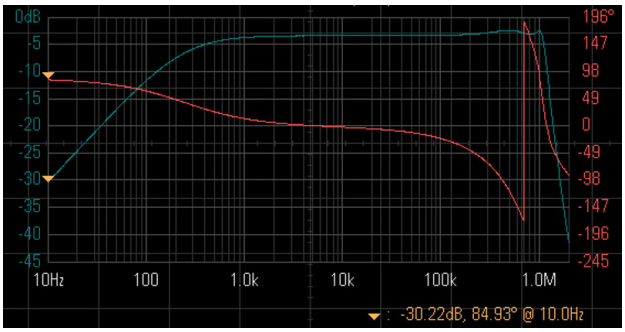

Fig. 10. 0.22 kHz–1 MHz filter Bode plot. The sampling kernel removes the dc component of the input signal. The magnitude (in blue) and phase (in red) are plotted on a logarithmic frequency scale.

sampler is depicted in Fig. 11. Fig. 12 presents an enlarged view focusing on specific features of the IF-TEM integrator transients, providing a detailed insight into the integration and sampling processes. The top right section displays an expanded view of the pulse center, highlighting the fast integrator reset mechanism. Notably, for the 1 s signal, the reset function operates on an ms scale, while for a 10 μs signal, the reset occurs on an ns scale. This reset functionality is crucial for ensuring accurate integration and sampling of signals with varying time scales. Furthermore, the figure demonstrates the operational linearity of the integrator, which is important for accurate signal recovery.

The primary IF-TEM components consist of the bias b, integrator, comparator, differentiator, and reset function. To guarantee sufficient samples for reconstruction, we should ensure that the δ threshold is achieved at least as many times as the desired sample amount. By adding the bias b to the input $y(t)$, the integrator obtains a signal that is always nonnegative. In this case, integration over a nonnegative signal is a positive function, and the threshold is always attained. For an FRI

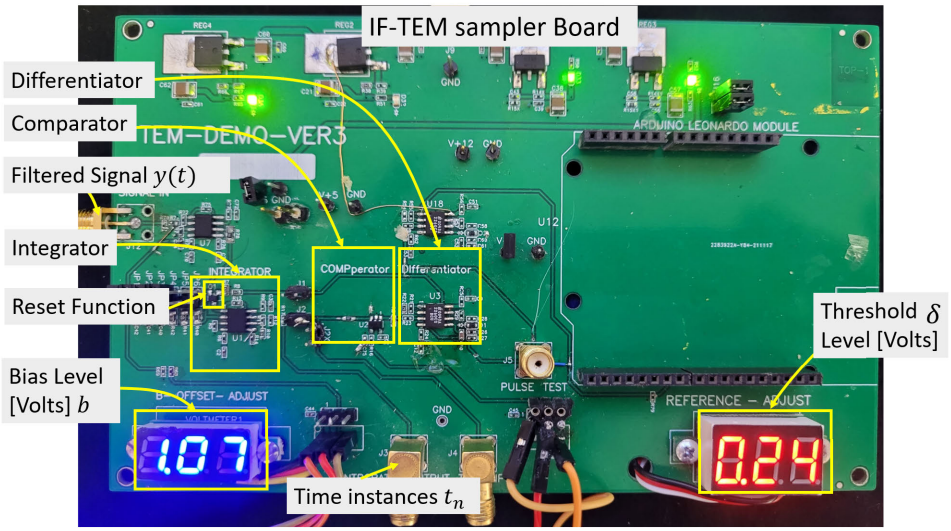

Fig. 11. IF-TEM hardware board.

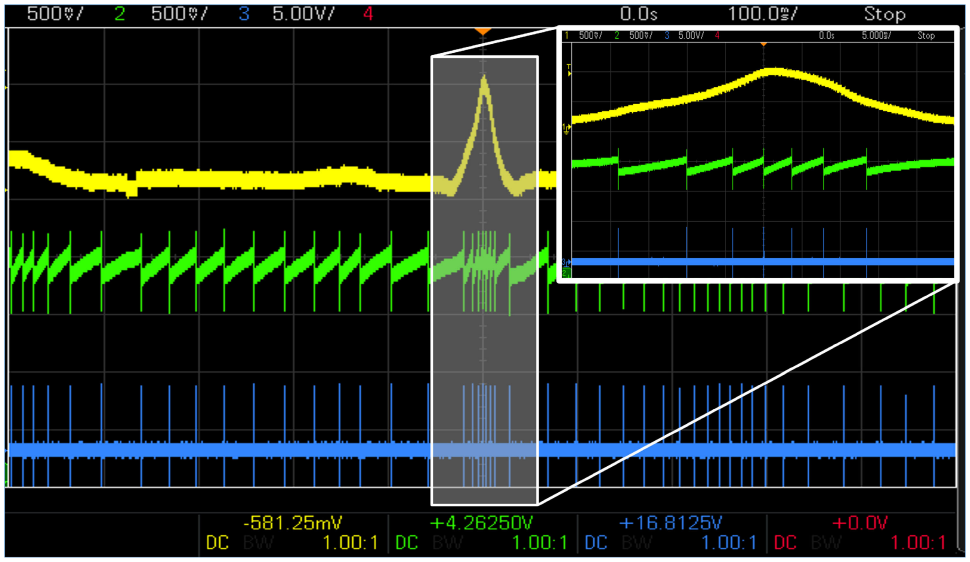

Fig. 12. Yellow depicts the 1-s input of IF-TEM, green shows the integrator output, and blue is the output time instances of IF-TEM. In the top right, an expanded view displays the pulse center along with the fast integrator reset mechanism.

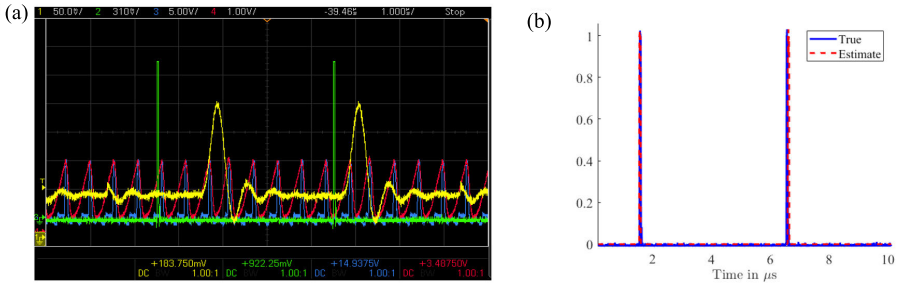

Fig. 13. (a) Original FRI signal $x(t)$ (green), the output of the BPF filter $y(t)$ (yellow), and the IF-TEM hardware resulted in 19 samples (blue). (b) IF-TEM hardware sampling and reconstruction: the input signal $x(t)$ (blue) alongside its reconstructed version (red).

signal $x(t)$ with L pulses, it can be shown that the sampler input filtered signal $y(t)$ is constrained by [21]

$$|y(t)| \leq c = L\ a_{\max}\ \|g\|_\infty \|h\|_1 \tag{28}$$

where g and h are the known filter and pulse shape, respectively. Consequently, the bias $b > c$, which is effectively a constant dc voltage, is selected manually using a potentiometer, which is a device that allows the user to adjust the electrical resistance in a circuit by turning a knob. By adjusting the resistance, the user can fine-tune the value of the bias to the desired level. It is important to carefully select the appropriate bias value to ensure that the IF-TEM system can function properly.

The output of the integrator is sent to the comparator, which compares the integrator voltage to a predefined threshold δ. The threshold is a constant dc voltage that is implemented

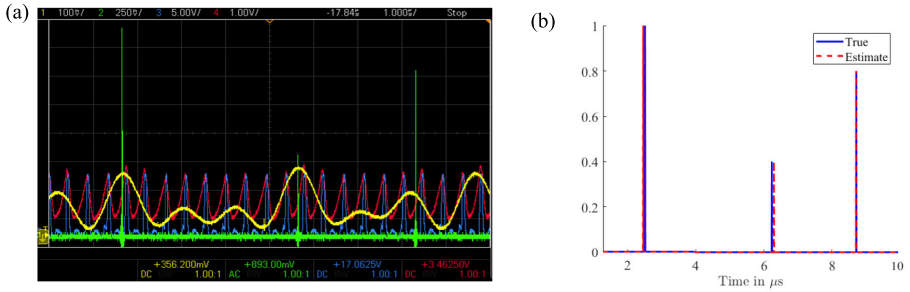

Fig. 14. (a) Original FRI signal $x(t)$ (green), the output of the BPF filter $y(t)$ (yellow), and the IF-TEM hardware resulted in 19 samples (blue). (b) IF-TEM hardware sampling and reconstruction: the input signal $x(t)$ (blue) alongside its reconstructed version (red).

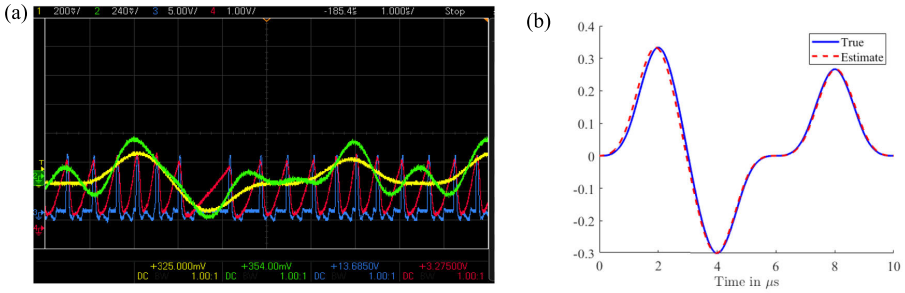

Fig. 15. (a) Original FRI signal $x(t)$ (green), the output of the BPF filter $y(t)$ (yellow), and the IF-TEM hardware resulted in 21 samples (blue). (b) IF-TEM hardware sampling and reconstruction: the input signal $x(t)$ (blue) alongside its reconstructed version (red).

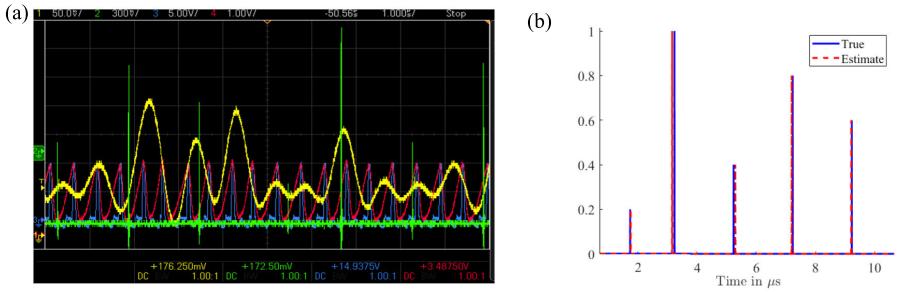

Fig. 16. (a) Original FRI signal $x(t)$ (green), the output of the BPF filter $y(t)$ (yellow), and the IF-TEM hardware resulted in 22 samples (blue). (b) IF-TEM hardware sampling and reconstruction: the input signal $x(t)$ (blue) alongside its reconstructed version (red).

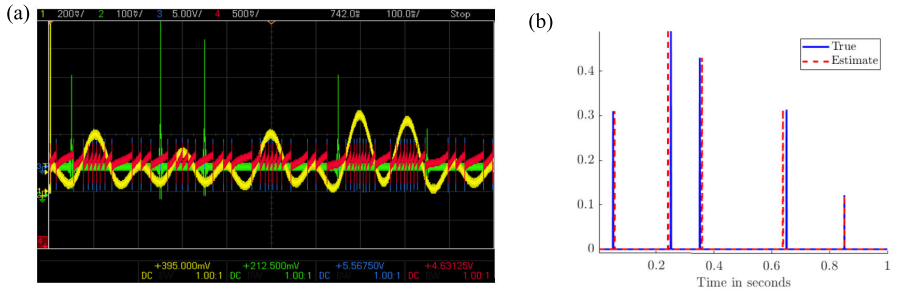

Fig. 17. (a) Original FRI signal $x(t)$ (green), the output of the BPF filter $y(t)$ (yellow), and the IF-TEM hardware resulted in 53 samples (blue). (b) IF-TEM hardware sampling and reconstruction: the input signal $x(t)$ (blue) alongside its reconstructed version (red).

in our hardware utilizing a potentiometer that is manually regulated and adjustable. The comparator is responsible for comparing the voltage produced by the integrator to a predefined threshold value. When the integrator voltage reaches or exceeds the threshold, the comparator's output changes. If the comparator's input is below the threshold, it will output a logical value of "0," while if the input is above the threshold, the output will be "1." In other words, the comparator will produce a sequence of logical "1" values when the integrator voltage hits the threshold. This change in the comparator's output signal indicates that the threshold has been reached and triggers the next stage in the IF-TEM process.

The output of the comparator is sent to the differentiator, which generates a short pulse that activates the fast reset function. This function is responsible for capturing the time instances t_n. The reset function consists of an amplifier and an FET that work together to quickly and completely discharge the integrator capacitor. In greater detail, the FET functions as a switch and is controlled by the pulse produced by the differentiator, which determines the duration of time that the FET is active. This allows the integrator capacitor to be fully

discharged. The FET has three terminals: a source, a gate, and a drain. By providing a voltage of "1" to the gate terminal, the FET can modify the conductivity between the drain and source terminals, which allows the current flow to be regulated. This results in a rapid and complete discharge of the integrator capacitor.

Since the IF-TEM sampler is an energy-efficient ASDM [11], acknowledged for its energy-efficient properties [11], [49], we focus our discussion on the TDC, which samples the filtered signal by capturing the successive differences in time instances. The proposed sampler combines the IF-TEM's analog sampling mechanism with a time-to-digital conversion, which can be used using an oscilloscope or a TDC, for end-to-end power-efficient sampling and digitization. The IF-TEM performs analog sampling by integrating the input signal and generating pulses at specific time instances, while the TDC converts these sampled time instances to the digital domain. TDCs offer a more energy-efficient alternative to traditional clock-based ADCs for the same number of samples, as they require fewer components and are not susceptible to clock drifting issues. The power savings of TDCs stem from their reduced component count and the ability to use a less accurate clock [50]. For example, as shown in Table II, a 12-bit TDC operating at 100 MHz in a 65-nm CMOS process consumes only 70 μW, while an 11-bit ADC with the same operating frequency and process consumes 2.4 mW, highlighting the significant power efficiency advantage of TDCs. In our case, with a signal containing $L = 5$ pulses, merely 22 time instances need to be captured. Given the minimal length between samples of approximately 0.4 μs, a clock frequency of 2.5 MHz suffices, resulting in a dedicated TDC consuming less than 70 μW for this example.

B. Circuit Challenges

To implement an IF-TEM circuit, it is necessary to employ an integrator that operates according to (2). Specifically, the integrator capacitor must operate in its linear domain, which is continuously charged or rising, as long as the input signal is positive. In addition, the IF-TEM thresholding process requires a fast reset mechanism (see Fig. 12). Therefore, our goal is to develop an integrator and reset function in which the capacitor of the integrator operates in its linear zone and discharges rapidly and completely. The main challenge in the implementation of the IF-TEM hardware is to design and implement such an IF-TEM integrator capacitor while supporting a wide range of input FRI signals without circuit modification. By utilizing the differentiator and an FET in the reset function, both the entire discharge and rapid discharge of the capacitor are accomplished for a variety of FRI signals. Next, we provide results from our hardware and compare them to our theoretical results from Theorem 1.

V. Hardware Experiments

To determine the proposed system's potential and feasibility, we performed experiments on the FRI-TEM hardware system we built. As depicted in Fig. 13(a), we consider an FRI input signal, referred to as $x(t)$, consisting of two pulses with a width of 100 ns and a delay of 5 μs between them. The sampling kernel mentioned in Section II-C was utilized in these experiments. The parameters for the IF-TEM circuit were set to a value of $\kappa = 3 \cdot 10^{-8}$, with a bias of $b = 3$ V and a threshold of $\delta = 1.5$ V. The specific time delays and amplitudes used in this input signal were chosen arbitrarily, and the IF-TEM parameters were selected to adhere to the constraints outlined in (15). As demonstrated in Fig. 13(a), the filtered signal $y(t)$ is forwarded to an IF-TEM sampler, which generated 19 time instances t_n, resulting in a firing rate of 1.9 MHz, which is 4.75 times the rate of innovation and 10.5 times the Nyquist rate. It is important to note that a minimum of $4L + 2 = 10$ time instances are required for off-grid reconstruction. Fig. 13(b) illustrates a comparison between the original input signal and the estimated signal. This demonstrates that the parameters of the FRI system can be robustly estimated while operating at a rate that is 10 times lower than the Nyquist rate.

In Figs. 14(a), 15(a), and 16(a), we demonstrate sampling and reconstruction of FRI signals with $L = 3, 5$ for $h(t)$ as a Dirac impulse and stream of pulses. The FRI signal is represented by the green curve, the filtered signal $y(t)$ is shown in yellow, and the time instances t_n produced by the IF-TEM sampler are depicted in blue. In each of these figures, the number of time instances produced is 19, 21, and 22, respectively, resulting in firing rates of 1.9, 2.1, and 2.2 MHz, which are all between 9.5 and 10.5 times the Nyquist rate. The reconstructed FRI signals are shown in Figs. 14(b), 15(b), and 16(b).

Fig. 17 demonstrates the sampling and recovery of an FRI signal with $L = 5$ for Dirac impulse $h(t)$ with $T = 1$ s. Fig. 18 presents a comparison between the reconstruction using the hardware measurements and the simulation for the delays of the FRI signals with (a) two pulses, (b) three pulses, and (c) five pulses. This comparison quantifies the performance of our proposed hardware prototype and reconstruction method by comparing the results obtained from the hardware average with those obtained from simulations.

TABLE I
List of Hardware Components

Device	Reference	Manufacturer
Inverter	AD8099	Analog Devices
Integrator	ADA4625	Analog Devices
Comparator	TLV3201	Texas Instruments
Differentiator + Amplifier	LT1364	Analog Devices
Reset Function	2N7002	Onsemi

TABLE II
Clock-Based ADC Versus TDC

Name	Technolodgy	Frequency	Power	Bits
ADC [51]	65nm CMOS	100MHz	$2.4mw$	11-bit
TDC [50]	65nm CMOS	100MHz	$70\mu w$	12-bits

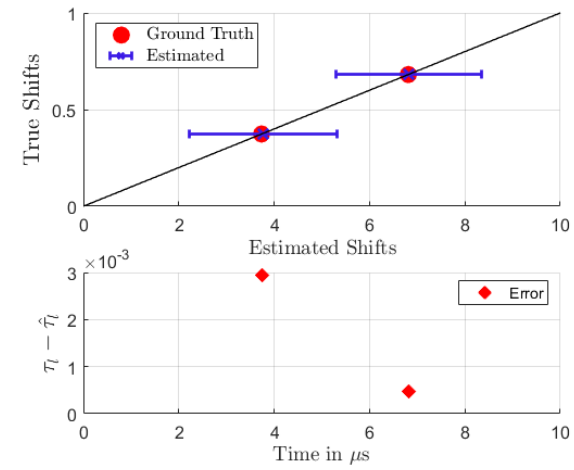

(a) $\sigma = 0.0193$ms

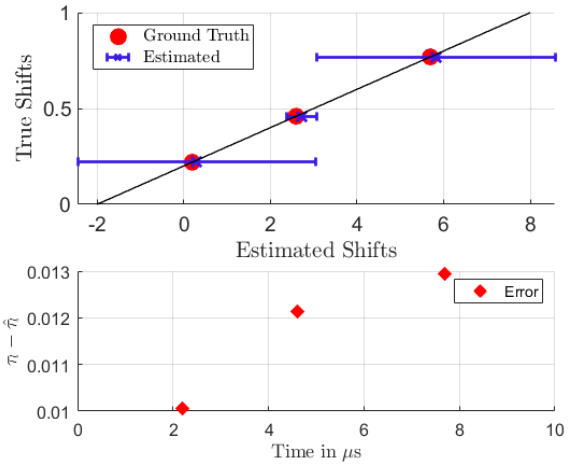

(b) $\sigma = 0.0352$ms

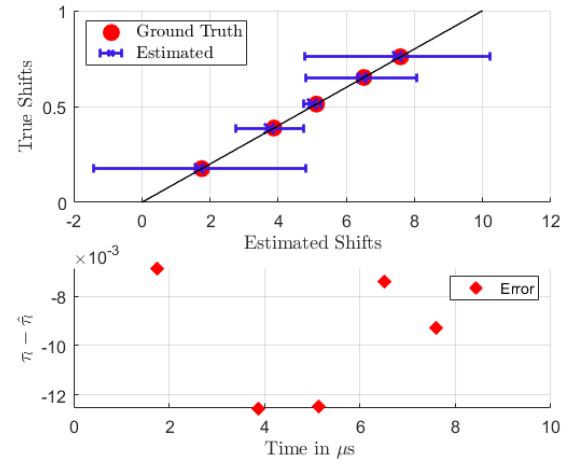

(c) $\sigma = 0.0173$ms

Fig. 18. Comparison of measured shifts from IF-TEM measurements compared to true shifts, across varying levels of jitter σ for (a) two pulses, (b) three pulses, and (c) five pulses. The jitter value represents the average of the measured shifts, with error bars denoting one standard deviation. Proximity to the 45° diagonal line reflects the effectiveness of recovery.

The evaluation involves calculating the average MSE between the reconstructed time shifts obtained from the hardware and simulation, as well as presenting the error bars that denote one standard deviation. The MSE is given in (27). This comparison provides insights into the accuracy and reliability of the hardware and reconstruction approach. In Fig. 19, we show the MSE of the signal reconstruction and the time shifts (27) as a function of the jitter σ. The error in the signal reconstruction and time delay estimation is found to be up to -25 and -70 dB, respectively. Both cases indicate accurate reconstruction. These results indicate that our proposed sampling and reconstruction method is suitable for radar and ultrasonic imaging applications.

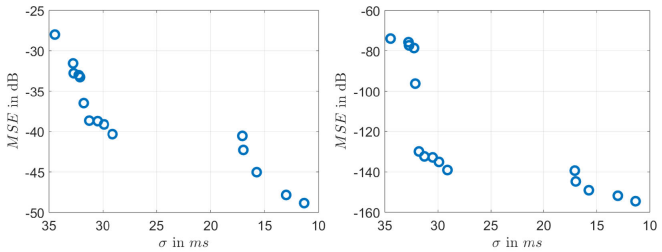

(a) (b)

Fig. 19. MSE as a function of the fluctuations σ. (a) Time shifts error. (b) Signal's reconstruction error.

VI. Conclusion

This research focused on FRI signal recovery using a time-based IF-TEM ADC. To address this challenge, we proposed a hardware prototype of a sub-Nyquist IF-TEM ADC and developed a robust reconstruction approach to accurately retrieve the FRI parameters. The hardware prototype that we introduced is an asynchronous, energy-efficient ADC that estimates the FRI parameters using a sub-Nyquist framework, which allows it to operate at rates significantly lower than the Nyquist rate. Our proposed hardware and reconstruction method has been demonstrated to successfully extract the FRI parameters, achieving reconstruction accuracy with errors not exceeding -25 dB. This performance is achieved while operating at sampling frequencies approximately one-tenth of the Nyquist rate. These results suggest that the proposed hardware prototype and reconstruction approach are effective and efficient in accurately recovering FRI signals and may be useful in various applications such as radar and ultrasonic imaging. The designed prototype characteristic and asynchronous operation make it particularly attractive for use in energy-constrained systems such as battery-powered devices where these factors are important considerations.

References

[1] H. Naaman, S. Mulleti, and Y. C. Eldar, "Uniqueness and robustness of tem-based FRI sampling," in *Proc. IEEE Int. Symp. Inf. Theory (ISIT)*, Jun. 2022, pp. 2631–2636.

[2] Y. C. Eldar, *Sampling Theory: Beyond Bandlimited System*. Cambridge, U.K.: Cambridge Univ. Press, 2015.

[3] M. Unser, "Sampling-50 years after Shannon," *Proc. IEEE*, vol. 88, no. 4, pp. 569–587, Apr. 2000.

[4] R. Piyare, A. L. Murphy, M. Magno, and L. Benini, "On-demand LoRa: Asynchronous TDMA for energy efficient and low latency communication in IoT," *Sensors*, vol. 18, no. 11, p. 3718, 2018.

[5] I. Shake, H. Takara, and S. Kawanishi, "Simple measurement of eye diagram and BER using high-speed asynchronous sampling," *J. Lightw. Technol.*, vol. 22, no. 5, pp. 1296–1302, May 2004.

[6] R. K. Siddharth, Y. B. N. Kumar, M. H. Vasantha, and E. Bonizzoni, "A low-power auxiliary circuit for level-crossing ADCs in IoT-sensor applications," in *Proc. IEEE Int. Symp. Circuits Syst. (ISCAS)*, May 2018, pp. 1–5.

[7] D. Kinniment and A. Yakovlev, "Low power, low noise micropipelined flash A–D converter," *IEE Proc.-Circuits, Devices Syst.*, vol. 146, no. 5, pp. 263–267, 1999.

[8] M. Rastogi, A. Singh Alvarado, J. G. Harris, and J. C. Príncipe, "Integrate and fire circuit as an ADC replacement," in *Proc. IEEE Int. Symp. Circuits Syst. (ISCAS)*, May 2011, pp. 2421–2424.

[9] F. Akopyan, R. Manohar, and A. B. Apsel, "A level-crossing flash asynchronous analog-to-digital converter," in *Proc. 12th IEEE Int. Symp. Asynchronous Circuits Syst. (ASYNC)*, Jun. 2006, p. 11.

[10] A. A. Lazar and L. T. Tóth, "Perfect recovery and sensitivity analysis of time encoded bandlimited signals," *IEEE Trans. Circuits Syst. I: Reg. Papers*, vol. 51, no. 10, pp. 2060–2073, Oct. 2004.

[11] A. S. Alvarado, M. Rastogi, J. G. Harris, and J. C. Príncipe, "The integrate-and-fire sampler: A special type of asynchronous $\Sigma - \Delta$ modulator," in *Proc. IEEE Int. Symp. Circuits Syst. (ISCAS)*, May 2011, pp. 2031–2034.

[12] E. Roza, "Analog-to-digital conversion via duty-cycle modulation," *IEEE Trans. Circuits Syst. II, Analog Digit. Signal Process.*, vol. 44, no. 11, pp. 907–914, Nov. 1997.

[13] D. Florescu and A. Bhandari, "Time encoding via unlimited sampling: Theory, algorithms and hardware validation," *IEEE Trans. Signal Process.*, vol. 70, pp. 4912–4924, 2022.

[14] D. Kościelnik and M. Miśkowicz, "Asynchronous sigma-delta analog-to digital converter based on the charge pump integrator," *Anal. Integr. Circuits Signal Process.*, vol. 55, no. 3, pp. 223–238, Jun. 2008.

[15] M. Miskowicz, "Efficiency of event-based sampling according to error energy criterion," *Sensors*, vol. 10, no. 3, pp. 2242–2261, Mar. 2010.

[16] N. Sayiner, H. V. Sorensen, and T. R. Viswanathan, "A level-crossing sampling scheme for A/D conversion," *IEEE Trans. Circuits Syst. II, Analog Digit. Signal Process.*, vol. 43, no. 4, pp. 335–339, Apr. 1996.

[17] A. Lazar, "Time encoding with an integrate-and-fire neuron with a refractory period," *Neurocomputing*, vols. 58–60, pp. 53–58, Jun. 2004.

[18] K. Adam, A. Scholefield, and M. Vetterli, "Multi-channel time encoding for improved reconstruction of bandlimited signals," in *Proc. IEEE Int. Conf. Acoust., Speech Signal Process. (ICASSP)*, May 2019, pp. 7963–7967.

[19] K. Adam, A. Scholefield, and M. Vetterli, "Sampling and reconstruction of bandlimited signals with multi-channel time encoding," *IEEE Trans. Signal Process.*, vol. 68, pp. 1105–1119, 2020.

[20] R. Alexandru and P. L. Dragotti, "Reconstructing classes of non-bandlimited signals from time encoded information," *IEEE Trans. Signal Process.*, vol. 68, pp. 747–763, 2020.

[21] H. Naaman, S. Mulleti, and Y. C. Eldar, "FRI-TEM: Time encoding sampling of finite-rate-of-innovation signals," *IEEE Trans. Signal Process.*, vol. 70, pp. 2267–2279, 2022.

[22] I. Maravic, M. Vetterli, and K. Ramchandran, "Channel estimation and synchronization with sub-Nyquist sampling and application to ultra-wideband systems," in *Proc. IEEE Int. Symp. Circuits Syst.*, vol. 5, May 2004, pp. 1–5.

[23] M. Davies et al., "Advancing neuromorphic computing with Loihi: A survey of results and outlook," *Proc. IEEE*, vol. 109, no. 5, pp. 911–934, May 2021.

[24] O. Simeone et al., "Learning algorithms and signal processing for brain-inspired computing [from the guest editors]," *IEEE Signal Process. Mag.*, vol. 36, no. 6, pp. 12–15, Nov. 2019.

[25] G. Nallathambi and J. C. Príncipe, "Integrate and fire pulse train automaton for QRS detection," *IEEE Trans. Biomed. Eng.*, vol. 61, no. 2, pp. 317–326, Feb. 2014.

[26] A. S. Alvarado, C. Lakshminarayan, and J. C. Principe, "Time-based compression and classification of heartbeats," *IEEE Trans. Biomed. Eng.*, vol. 59, no. 6, pp. 1641–1648, Jun. 2012.

[27] G. Gallego et al., "Event-based vision: A survey," *IEEE Trans. Pattern Anal. Mach. Intell.*, vol. 44, no. 1, pp. 154–180, Jan. 2020.

[28] P. Lichtsteiner, C. Posch, and T. Delbruck, "A 128×128 120 dB 15 μs latency asynchronous temporal contrast vision sensor," *IEEE J. Solid-State Circuits*, vol. 43, no. 2, pp. 566–576, Jan. 2008.

[29] H. Rebecq, R. Ranftl, V. Koltun, and D. Scaramuzza, "Events-to-video: Bringing modern computer vision to event cameras," in *Proc. IEEE/CVF Conf. Comput. Vis. Pattern Recognit. (CVPR)*, Jun. 2019, pp. 3857–3866.

[30] K. Adam, "A time encoding approach to training spiking neural networks," in *Proc. IEEE Int. Conf. Acoust., Speech Signal Process. (ICASSP)*, May 2022, pp. 5957–5961.

[31] D. Gontier and M. Vetterli, "Sampling based on timing: Time encoding machines on shift-invariant subspaces," *Appl. Comput. Harmon. Anal.*, vol. 36, no. 1, pp. 63–78, Jan. 2014.

[32] S. Rudresh, A. J. Kamath, and C. S. Seelamantula, "A time-based sampling framework for finite-rate-of-innovation signals," in *Proc. IEEE Int. Conf. Acoust., Speech Signal Process. (ICASSP)*, May 2020, pp. 5585–5589.

[33] M. Hilton, R. Alexandru, and P. L. Dragotti, "Time encoding using the hyperbolic secant kernel," in *Proc. 28th Eur. Signal Process. Conf. (EUSIPCO)*, Jan. 2021, pp. 2304–2308.

[34] M. Vetterli, P. Marziliano, and T. Blu, "Sampling signals with finite rate of innovation," *IEEE Trans. Signal Process.*, vol. 50, no. 6, pp. 1417–1428, Jun. 2002.

[35] J. Castorena and C. D. Creusere, "Sampling of time-resolved full-waveform LIDAR signals at sub-Nyquist rates," *IEEE Trans. Geosci. Remote Sens.*, vol. 53, no. 7, pp. 3791–3802, Jul. 2015.

[36] R. Tur, Y. C. Eldar, and Z. Friedman, "Innovation rate sampling of pulse streams with application to ultrasound imaging," *IEEE Trans. Signal Process.*, vol. 59, no. 4, pp. 1827–1842, Apr. 2011.

[37] N. Wagner, Y. C. Eldar, and Z. Friedman, "Compressed beamforming in ultrasound imaging," *IEEE Trans. Signal Process.*, vol. 60, no. 9, pp. 4643–4657, Sep. 2012.

[38] S. Mulleti, S. Nagesh, R. Langoju, A. Patil, and C. S. Seelamantula, "Ultrasound image reconstruction using the finite-rate-of-innovation principle," in *Proc. IEEE Int. Conf. Image Process. (ICIP)*, Oct. 2014, pp. 1728–1732.

[39] O. Bar-Ilan and Y. C. Eldar, "Sub-Nyquist radar via Doppler focusing," *IEEE Trans. Signal Process.*, vol. 62, no. 7, pp. 1796–1811, Apr. 2014.

[40] W. U. Bajwa, K. Gedalyahu, and Y. C. Eldar, "Identification of parametric underspread linear systems and super-resolution radar," *IEEE Trans. Signal Process.*, vol. 59, no. 6, pp. 2548–2561, Jun. 2011.

[41] T. Blu, H. Bay, and M. Unser, "A new high-resolution processing method for the deconvolution of optical coherence tomography signals," in *Proc. IEEE Int. Symp. Biomed. Imag.*, Jul. 2002, pp. 777–780.

[42] P. L. Dragotti, M. Vetterli, and T. Blu, "Sampling moments and reconstructing signals of finite rate of innovation: Shannon meets strang–fix," *IEEE Trans. Signal Process.*, vol. 55, no. 5, pp. 1741–1757, May 2007.

[43] S. Mulleti and C. S. Seelamantula, "Paley–Wiener characterization of kernels for finite-rate-of-innovation sampling," *IEEE Trans. Signal Process.*, vol. 65, no. 22, pp. 5860–5872, Nov. 2017.

[44] H. Naaman, S. Mulleti, Y. C. Eldar, and A. Cohen, "Time-based quantization for FRI and bandlimited signals," in *Proc. 30th Eur. Signal Process. Conf. (EUSIPCO)*, 2022, pp. 2241–2245.

[45] M. Rastogi, V. Garg, and J. G. Harris, "Low power integrate and fire circuit for data conversion," in *Proc. IEEE Int. Symp. Circuits Syst.*, May 2009, pp. 2669–2672.

[46] A. A. Lazar and L. T. Toth, "Time encoding and perfect recovery of bandlimited signals," in *Proc. IEEE Int. Conf. Acoust., Speech, Signal Process. (ICASSP)*, vol. 1, Apr. 2003, p. 709.

[47] Y. Barbotin, A. Hormati, S. Rangan, and M. Vetterli, "Estimation of sparse MIMO channels with common support," *IEEE Trans. Commun.*, vol. 60, no. 12, pp. 3705–3716, Dec. 2012.

[48] I. L. Newberg, C. M. Gee, G. D. Thurmond, and H. W. Yen, "Long microwave delay fiber-optic link for radar testing," *IEEE Trans. Microw. Theory Techn.*, vol. 38, no. 5, pp. 664–666, May 1990.

[49] I. Bilinskis, *Digital Alias-Free Signal Processing*. Hoboken, NJ, USA: Wiley, 2007.

[50] A. Naguib, "High speed and low power comparator in 65 nm CMOS for energy efficient biomedical SAR ADCs," in *Proc. 12th Int. Conf. Electr. Eng. (ICEENG)*, Jul. 2020, pp. 339–342.

[51] Y.-H. Chung and C.-W. Yen, "An 11-bit 100-MS/s subranged-SAR ADC in 65-nm CMOS," *IEEE Trans. Very Large Scale Integr. (VLSI) Syst.*, vol. 25, no. 12, pp. 3434–3443, Dec. 2017.